AUTOTAXIN/LYSOPHOSPHOLIPASE D-MEDIATED LPA SIGNALING IS REQUIRED TO FORM DISTINCTIVE LARGE LYSOSOMES IN THE VISCERAL ENDODERM CELLS OF THE MOUSE YOLK SAC

Seiichi Koike[1], Kazuko Keino-Masu[1], Tatsuyuki Ohto[1,2], Fumihiro Sugiyama[3], Satoru Takahashi[3], and Masayuki Masu[1]*

From [1]Department of Molecular Neurobiology, Institute of Basic Medical Sciences, and [2]Department of Pediatrics, Institute of Clinical Medicine, Graduate School of Comprehensive Human Sciences, and [3]Laboratory Animal Resource Center, University of Tsukuba, 1-1-1 Tennoudai, Tsukuba, Ibaraki 305-8577, Japan

Running title: Autotaxin-LPA signaling in lysosome biogenesis

Address correspondence to: Masayuki Masu, 1-1-1 Tennoudai, Tsukuba, Ibaraki 305-8577, Japan; Tel: +81-29-853-3249; Fax: +81-29-853-3498; E-mail: mmasu@md.tsukuba.ac.jp

Autotaxin, a lysophospholipase D encoded by the *Enpp2* gene, is an exoenzyme that produces lysophosphatidic acid in the extracellular space. Lysophosphatidic acid acts on specific G protein-coupled receptors, thereby regulating cell growth, migration, and survival. Previous studies have revealed that *Enpp2*$^{-/-}$ mouse embryos die at about E9.5 owing to angiogenic defects in the yolk sac. However, what cellular defects occur in *Enpp2*$^{-/-}$ embryos and what intracellular signaling pathways are involved in the phenotype manifestation remain unknown. Here, we show that *Enpp2* is required to form distinctive large lysosomes in the yolk sac visceral endoderm cells. From E7.5 to E9.5, *Enpp2* mRNA is abundantly expressed in the visceral endoderm cells. In *Enpp2*$^{-/-}$ mouse embryos, lysosomes in the visceral endoderm cells are fragmented. By using a whole embryo culture system combined with specific pharmacological inhibitors for intracellular signaling molecules, we show that lysophosphatidic acid receptors and the Rho-ROCK-LIM kinase pathway are required to form large lysosomes. In addition, electroporation of dominant negative forms of Rho, ROCK, or LIM kinase also leads to the size reduction of lysosomes in wild-type VE cells. In *Enpp2*$^{-/-}$ visceral endoderm cells, the steady-state levels of cofilin phosphorylation and actin polymerization are reduced. In addition, perturbations of actin turnover dynamics by actin inhibitors cytochalasin B and jasplakinolide result in the defect in lysosome formation. These results suggest that constitutive activation of the Rho-ROCK-LIM kinase pathway by extracellular production of lysophosphatidic acid by the action of autotaxin is required to maintain large size of lysosomes in visceral endoderm cells.

Autotaxin, also known as ENPP2 (ectonucleotide pyrophosphatase/phosphodiesterase 2), is an extracellular lysophospholipase D (lysoPLD) that produces lysophosphatidic acid (LPA) (1-4). LPA is a lipid mediator possessing a wide variety of biological functions, including cell proliferation, migration, and survival (4-6). LPA activates LPA_{1-6} receptors, which are coupled to several downstream signals via at least 3 distinct G protein subfamilies: $G_{12/13}$, G_i, and G_q (4, 5, 7). Additionally, the role of autotaxin in sphingosine 1-phosphate (S1P) production was suggested in vitro, but remains to be established in vivo (4, 8). Recently, it has been reported that *Enpp2*$^{-/-}$ mice died

at embryonic day 9.5 (E9.5) owing to angiogenic defects in the yolk sac (9, 10). *Enpp2*$^{-/-}$ embryos also showed allantois malformation, neural tube defects, no axial turning, and head enlargement, indicating the essential roles of *Enpp2* for mouse embryonic development (9, 10). Furthermore, adult *Enpp2*-heterozygous mice showed half-normal levels of lysoPLD activity and LPA, but normal levels of S1P, in plasma, suggesting that autotaxin is a major LPA-producing enzyme in vivo (9, 10). However, what cellular defects are caused by the lack of LPA production in *Enpp2*$^{-/-}$ embryos and what signaling pathways underlie the defects remain elusive.

The extraembryonic visceral yolk sac is the first place where hematopoiesis and vasculogenesis occur in the mouse. It is composed of two layers, the visceral endoderm (VE) and the underlying mesoderm layers. VE cells play a critical role in the maternofetal exchange of nutrients prior to the establishment of a chorioallantoic placenta (~E9). They endocytose maternal proteins vigorously, hydrolyze the proteins in lysosomes, and supply the resultant products to the developing embryo (11, 12). Reflecting high endocytic and digestive activity, VE cells are endowed with dinstinctively large lysosomes (known as amorphous vacuoles in electron microscopy) (11, 12). Blockade of VE cell functions using chemicals, antibodies, or gene disruption caused fetal malformation (11, 13), suggesting the functional importance of VE cells in rodent development.

Lysosomes are dynamic membrane-bound organelles that receive and degrade macromolecules from endocytic, phagocytic, and autophagic pathways (14, 15). They undergo dynamic fusion/fission and yet cells maintain a relatively constant size and number of lysosomes (14, 15). Genetic studies in yeast and *Drosophila* as well as cell biological studies in mammalian cells have identified many intracellular components involved in the biogenesis of lysosomes and vacuoles (yeast homologs of lysosomes) and elucidated their functions (14, 15). However, it remains unknown whether lysosome biogenesis is regulated by extracellular signals and which signaling pathway(s), if any, regulate the process.

In the present study, we show that *Enpp2* mRNA is highly expressed in the yolk sac VE cells from E7.5 to E9.5. In the VE cells of *Enpp2*$^{-/-}$ embryos, distinctive large lysosomes are fragmented. When embryos are cultured in the presence of pharmacological inhibitors for the LPA receptors, Rho, ROCK/Rho kinase, or LIM kinase (LIMK), these drugs induce lysosomal defects similar to those observed in *Enpp2*$^{-/-}$ VE cells. In addition, inhibition of Rho, ROCK, or LIMK by electroporating their dominant negative forms or activation of cofilin by electroporating its constitutive active form into wild-type embryos induces the size reduction of lysosomes in VE cells. In *Enpp2*$^{-/-}$ VE cells, the steady-state levels of cofilin phosphorylation and actin polymerization are reduced. Moreover, perturbations of actin turnover dynamics by cytochalasin B or jasplakinolide result in the defect in lysosome formation in VE cells. These findings suggest that the control of actin turnover dynamics through the Rho-ROCK-LIMK pathway by way of autotaxin-LPA signaling is required for the regulatory processes of lysosome biogenesis.

EXPERIMENTAL PROCEDURES

Animal Experiments—All the experiments using animals were approved by the Animal Care and Use Committee of the University of Tsukuba and performed under its guidelines. Noon of the day on which a vaginal plug was observed was taken as embryonic day 0.5 (E0.5). Time pregnant ICR mice (CLEA Japan, Tokyo, Japan: Japan SLC, Hamamatsu, Japan) were used for pharmacological experiments and electroporation.

Generation of *Enpp2*-deficient Mice—A gene-targeting vector was constructed by inserting the mouse genomic DNA fragments flanking exons 6 and 7 of the *Enpp2* gene into a TC3 vector (a gift from Dr. Ryoichiro Kageyama, Kyoto University, Japan), which contained a cassette of

stop-IRES-lacZ-polyA, a neomycin-resistant gene, and a diphtheria toxin A fragment gene. The linearized vector was electroporated into mouse ES cells (E14 clone derived from 129/Ola), and neomycin-resistant colonies were selected by PCR. Whether homologous recombination occurred correctly in the selected clones was confirmed using Southern blotting with 3' and 5' probes. Chimeric mice, obtained by injecting the ES cells into C57BL/6J blastocysts, were mated with wild-type C57BL/6N mice. Offspring generated by intercrosses of heterozygotes (F1 generation) were used. Mice were genotyped by duplex PCR using the primers,
5'-CTGCTGAAACTTAATGCACTGGAC-3' (*Enpp2* forward),
5'-TGTGTAAGTCAGGGAACAACTCTG-3' (*Enpp2* reverse),
and 5'-TGCTCCAGACTGCCTTGGGAAAAG-3' (*neo*). Fragments of 473 and 336 bp were amplified from the wild-type and targeted alleles, respectively.

Collection of Extraembryonic Coelomic Fluid (ECF) and Western Blotting—ECF was aspirated by using a fine-tip glass needle; about 1 μl of ECF was obtained from one E8.5 embryo. ECF collected from 3 to 5 mouse embryos was used for western blotting with anti-autotaxin ATX-N1 (1:1,000, TransGenic, Kumamoto, Japan; described previously in ref. 16). The signal was detected using horse radish peroxidase (HRP)-conjugated anti-rabbit IgG (1:10,000; Bio-Rad, Hercules, CA, USA) and ECL PLUS Western Blotting Detection Reagents (GE Healthcare Bio-Sciences Corp., Piscataway, NJ, USA).

Histological Analysis—In situ hybridization and immunohistochemistry were performed as described previously (16). Primary antibodies used were rabbit polyclonal anti-cofilin and anti-phosphorylated cofilin (1:400; a kind gift of Dr. Kensaku Mizuno, Tohoku University, Japan), rat monoclonal anti-E-cadherin (1:1,000; a kind gift of Dr. Shinji Hirano, Kochi University, Japan), rat monoclonal anti-LAMP1 (1:500; Developmental Studies Hybridoma Bank, Iowa city, IA, USA), and HRP-conjugated anti-mouse IgG (1:1,000; Chemicon, Temecula, CA, USA). The secondary antibodies used were Cy3-labeled anti-rabbit IgG (1:500; Jackson ImmunoResearch), Alexa488-conjugated anti-rat IgG (1:1,000; Invitrogen, Carlsbad, CA, USA) and Cy3-labeled anti-rat IgG (1:1000; Jackson ImmunoResearch). Fluorescent images were obtained using a laser scanning confocal microscope (LSM510; Carl Zeiss, Jena, Germany).

RT-PCR—Total RNA was isolated from yolk sacs of E7.0 to E12.5 mice using Sepasol I (Nacalai Tesque, Kyoto, Japan). Reverse transcription and PCR were performed using oligo(dT)$_{12\text{-}18}$, Superscript II reverse transcriptase (Invitrogen), and AmpliTaq Gold (Applied Biosystems, Foster City, CA, USA). The PCR primers used were 5'-GGTCAATAGCATGCAGACTG-3' (forward) and 5'-ACAGTTGGTCAGGTGTTCTG-3' (reverse) for *Enpp2*, and 5'-CAGGGCTGCCATTTGCAGTG-3' (forward) and 5'-TGGGGTCTCGCTCCTGGAAG-3' (reverse) for *Gapdh*.

Electron Microscopy—E8.5 mouse embryos were fixed in 2.5% glutaraldehyde in phosphate-buffered saline (PBS) at 4°C overnight. Tissues were postfixed in buffered osmium tetroxide and embedded in epoxy according to standard procedures. Ultrathin sections, counterstained with uranyl acetate and lead citrate, were examined using a transmission electron microscope (H7000; Hitachi, Tokyo, Japan) operated at 75 kV.

Imaging of Intracellular Vesicles—Whole embryos with intact yolk sacs, dissected at E8.5 or cultured for 1 day from E7.5, were incubated with 100 nM LysoTracker Red (Invitrogen) in Dulbecco's modified Eagle Medium (DMEM) at 37°C for 5 min. Whole embryos were then mounted on a glass-bottom dish (Matsunami, Osaka, Japan), allowing observation of the yolk sac using a laser scanning confocal microscope (LSM510; Zeiss) at room temperature. The areas of lysosomes were measured using Image J software. The average size of lysosomes was

obtained from each embryo, and compared and statistically analyzed between different experiment conditions.

Ex Vivo Whole Embryo Culture—Whole embryo culture was performed as described previously (17, 18). In brief, embryos were dissected at E7.5 and cultured in 100% rat serum (Charles River, Yokohama, Japan) supplemented with 2 mg/ml glucose in a culture bottle placed in a rotation drum culture system (Ikemoto Rika, Tokyo, Japan) in 5% O_2, 5% CO_2, and 90% N_2 at 37°C for 24 h. In pharmacological experiments, embryos were incubated with the following reagents: 3-(4-[4-([1-(2-chlorophenyl)ethoxy]carbonyl amino)-3-methyl-5-isoxazolyl] benzylsulfanyl)propanoic acid (Ki16425), 10 μM (Sigma-Aldrich, St. Louis, MO, USA); (R)-phosphoric acid mono-[2-amino-2-(3-octyl-phenylcarbamoyl)-ethyl] ester (VPC 23019), 10 μM (Avanti Polar Lipid, Alabaster, AL, USA); exoenzyme C3 (*Clostridium botulinum*), 20 μg/ml (Calbiochem, Darmstadt, Germany); (S)-(+)-2-methyl-1-[(4-methyl-5-isoquinolynyl)sulfonyl]homopiperazine dihydrochloride (H1152), 0.1 μM (Calbiochem); 1-[6-[[(17β)-3-methoxyestra-1,3,5(10)-trien-17-yl]amino]hexyl]-1H-pyrrole-2,5-dione (U-73122), 10 μM (Sigma-Aldrich); 2-(4-morpholinyl)-8-phenyl-1(4H)-benzopyran-4-one hydrochloride (LY294002), 10 μM (Sigma-Aldrich); pertussis toxin, 0.5 μg/ml (Calbiochem); 2-(2'-amino-3'-methoxy)-flavone (PD98059), 10 μM (Calbiochem); (R)-(+)-*trans*-N-(4-pyridyl)-4-(1-aminoethyl)-cyclohexanecarboxamide, 2HCl (Y-27632), 0.1-1 μM (Calbiochem); 1-(1-hydroxy-5-isoquinolinesulfonyl)homopiperazine monohydrochloride (Hydroxyfasudil), 1-10 μM (Sigma-Aldrich); 1-phenyl-1,2,3,4-tetrahydro-4-hydroxypyrrolo[2.3-*b*]-7-methylquinolin-4-one (blebbistatin), 10 μM (Toronto Research Chemicals, North York, On, Canada); cytochalasin B, 0.3 μM (Calbiochem); jasplakinolide, 10 nM (Calbiochem); S3 and RV peptides, 15 μg/ml (a kind gift of Dr. Kensaku Mizuno, Tohoku University).

Phalloidin Staining and Quantitation—For phalloidin staining, embryos were fixed with 4% paraformaldehyde in PBS at 37°C for 15 min. Whole embryos or cryostat sections were incubated with 0.2 U/ml Alexa488- or Alexa-546-conjugated phalloidin (Invitrogen) for 60 min. To compare fluorescence signal intensity, confocal images of yolk sacs in cryostat sections were collected with all laser settings constant. Fluorescence signal intensity was obtained using Zeiss LSM510 software and analyzed statistically using the t-test.

Electroporation of Whole Embryos—Whole embryos were dissected at E7.5 and transferred to Hanks' Balanced Salt Solution (HBSS; Invitrogen) kept at 37°C. One embryo was inserted into a small hole of an agarose mold (2% agarose/PBS, 7 mm square) placed in HBSS. The solution bathing the embryos was then replaced with HBSS containing 2 mg/ml DNA. Three square electric pulses (30 V, 50 ms duration, 1 pulse/s) were delivered to the agarose mold using an electroporator (CUY21; Nepa Gene, Chiba, Japan) and a 10-mm electrode (CUY650P10; Nepa Gene). After electroporation, the embryo was rinsed with HBSS and cultured as described in the previous section. Dominant negative (DN) and constitutive active (CA) forms of RhoB, ROCK, LIMK, and cofilin were kind gifts of Dr. Toshio Hirano (Osaka University), Dr. Shu Narumiya (Kyoto University), and Dr. Kensaku Mizuno (Tohoku University). DN-RhoB [RhoB (T19N)] and CA-RhoB [RhoB (G14V)] (19) were subcloned into the pEGFP-IRES2 vector (Clontech, Mountain View, CA, USA). DN-ROCK (KD-IA) and CA-RCOK (Δ3) (20) in the pCAGGS expression vector were fused to EGFP at their N-termini. DN-LIMK [LIMK1 (D460A)] and CA-LIMK [LIMK1 (T508EE)] (21) were subcloned into the pEGFP-IRES2 vector. DN-cofilin [cofilin (S3E)] and CA-cofilin [cofilin (S3A)] (22,23) were fused to YFP at their N-termini in the expression vector derived from pEGFP-C1 (Clontech).

RESULTS

Formation of Large Lysosomes is Impaired in *Enpp2*$^{-/-}$ VE Cells—*Enpp2* knockout mice were generated by disrupting the exons that encode the enzyme catalytic domain (Fig. 1A and B). *Enpp2* mRNA and protein were completely absent in *Enpp2*$^{-/-}$ mice (Fig. 1C and D). Whilst heterozygous mice were apparently normal and fertile, *Enpp2*$^{-/-}$ embryos died at E9.5 owing to angiogenic defects in the yolk sac (Fig. 1E and F), as reported previously (9, 10). To elucidate the roles of *Enpp2* in early development, its expression before E9.5 was examined. *Enpp2* mRNA was first detectable in the embryonic ectoderm at the late cylinder and primitive streak stages (E6.0 to E6.5) (Fig. 2A). From E7.5 to E8.5, strong signals were detected in the yolk sac, especially in VE cells (Fig. 2A). RT-PCR indicated that *Enpp2* mRNA was highly expressed in the yolk sac between E7.5 and E9.5 (Fig. 2B).

Thus, we focused on yolk sac VE cells. While searching for possible defects using immunohistochemistry, we noticed intriguing changes in the intracellular vesicles in *Enpp2*$^{-/-}$ VE cells. Because VE cells vigorously take up maternal proteins including IgG from the apical surface, endocytic vesicles can be visualized simply by immunostaining for mouse IgG. Control VE cells had large IgG-containing vesicles, whereas *Enpp2*$^{-/-}$ VE cells had smaller punctate vesicles (Fig. 3A, top). Electron microscopy demonstrated that control VE cells had a few large vesicles in the apical portion, whereas *Enpp2*$^{-/-}$ VE cells had numerous smaller vesicles (Fig. 3A, middle). To examine lysosomes in VE cells, we stained whole embryos with LysoTracker Red, a fluorescent dye that selectively accumulates in acidic organelles, and observed lysosomes in VE cells using a confocal microscope. This analysis revealed that lysosomes became significantly smaller and the number of lysosomes significantly increased in *Enpp2*$^{-/-}$ VE cells (Fig. 3A-B). Similarly, immunostaining with a lysosome marker, LAMP1, also revealed that lysosomes were smaller in *Enpp2*$^{-/-}$ VE cells (Fig. S1). These findings indicate that *Enpp2*$^{-/-}$ embryos had defects in the formation of large lysosomes, which are one of the distinctive features of VE cells.

LPA Receptors are Required to Form Large Lysosomes in VE Cells—We next examined the downstream signaling pathways of autotaxin using an ex vivo whole embryo culture system. Whole embryo culture is a well-established system that has been proved to be useful for studying normal development as well as assessing teratogenicity and gene functions (17, 18). When E7.5 wild-type embryos were cultured for 1 day, the appearances of the yolk sac and embryos were indistinguishable from those of the in-utero-grown E8.5 wild-type embryos (Fig. S2A). In addition, when E7.5 *Enpp2*$^{-/-}$ embryos were cultured for 1 day, head cavity was formed as seen in the in-utero-grown E8.5 *Enpp2*$^{-/-}$ embryos (Fig. S2A). Furthermore, the lysosome size in VE cells was reduced in the cultured *Enpp2*$^{-/-}$ embryos compared with that in the cultured wild-type embryos, in the same way and to the same extent that the lysosome size in VE cells was reduced in the *Enpp2*$^{-/-}$ embryos in vivo (Fig. S2A-B). These results indicate that a whole embryo culture system faithfully mimics in vivo development of wild-type and *Enpp2*$^{-/-}$ embryos, thus providing a feasible tool to test the effects of pharmacological manipulation of VE cells.

We thus set out to test the effects of the inhibitors of the LPA signaling pathway. In this study, we used subtoxic concentrations of drugs, which were carefully predetermined in preliminary tests as not inducing developmental retardation or cardiac arrest (data not shown). First, LPA and S1P receptor antagonists were tested. When E7.5 wild-type embryos were cultured for 1 day with 10 μM Ki16425, an LPA_1/LPA_3 antagonist (24), lysosomes became significantly smaller (Fig. 4A-B). In contrast, 10 μM VPC23019, an $S1P_1/S1P_3$ antagonist (25), did not induce size reduction of lysosomes (Fig. 4A-B), although the drug must have effectively acted on the yolk sac because it induced angiogenic defects (data not shown). These

findings indicate that LPA receptor signaling is required to form large lysosomes in VE cells.

Rho-ROCK Pathway is Required to Form Large Lysosomes in VE Cells—LPA receptors are coupled to several signaling pathways through distinct G proteins; the major pathways include $G_{12/13}$-Rho-ROCK, G_i-phosphatidylinositol 3-kinase (PI3K)-Rac, G_i-Ras-MAPK, and G_q-phospholipase C (PLC) (4, 5, 7). To determine which pathway is required in the downstream of autotaxin, we tested selective inhibitors for each pathway. Treatment of embryos with either a Rho inhibitor, *Clostridium* C3 exoenzyme (20 μg/ml), or a ROCK inhibitor, H1152 (0.1 μM), resulted in a significant size reduction of lysosomes (Fig. 4C, Fig. S3A). Other ROCK inhibitors, hydroxyfasudil (1-10 μM) and Y-27632 (1 μM), were also effective (Fig. S4). In contrast, none of the inhibitors of G_i (pertussis toxin, 0.5 μg/ml), PLC (U-73122, 10 μM), PI3K (LY294002, 10 μM), or MAPK (PD98059, 10 μM) had any effect on the size of lysosomes (Fig. 4C, Fig. S3A). These findings indicate that the Rho-ROCK pathway plays an important role in the downstream of autotaxin-LPA signaling in the formation of large lysosomes in VE cells.

LIMK Pathway is Required to Form Large Lysosomes in VE Cells—The main downstream targets of ROCK are LIMK and myosin light chain (MLC). ROCK phosphorylates and activates LIMK, which in turn phosphorylates and inactivates cofilin, a protein that stimulates actin filament disassembly (23, 26, 27). ROCK also induces MLC phosphorylation directly and indirectly through the inhibition of myosin phosphatase by phosphorylating its myosin-binding subunit (28). We tested which pathway is the main target of ROCK in this system. When mouse embryos were cultured with a myosin II inhibitor, blebbistatin (10 μM), the lysosome size was not changed (Fig. 4D, Fig. S3B). Thus, we next examined the effect of a cell-permeable LIMK inhibitor, S3 peptide, which contains the N-terminal 16 amino acid sequence of cofilin and the cell-permeable sequence of penetratin (29). As a negative control, RV peptide, which contains the reverse sequence of cofilin and the cell-permeable sequence of penetratin, was used (29). When mouse embryos were cultured with 15 μg/ml of S3 or RV peptide, S3 peptide inhibited cofilin phosphorylation (Fig. S5) and resulted in the size reduction of lysosomes in VE cells (Fig. 4E, Fig. S3B). These findings indicate that the LIMK-cofilin pathway is the main target of ROCK and responsible for the formation of large lysosomes in VE cells.

If LIMK activity is reduced in *Enpp2*$^{-/-}$ VE cells, it would be expected to decrease phosphorylation of cofilin (23, 26, 27). We thus examined phosphorylation levels of cofilin by immunostaining of VE cells with anti-phosphorylated cofilin or anti-total-cofilin antibody. Quantitation of the staining intensity revealed that the steady-state level of cofilin phosphorylation was significantly decreased without affecting the cofilin levels in *Enpp2*$^{-/-}$ VE cells (Fig. 5A-B). This finding of decreased cofilin phosphorylation strongly supports the supposition that LIMK activity was decreased in *Enpp2*$^{-/-}$ VE cells.

Actin Filaments are Depolymerized in *Enpp2*$^{-/-}$ VE Cells—Reduced phosphorylation of cofilin activates cofilin, thereby leading to depolymerization and severance of the actin filaments (27). To examine whether this happens in *Enpp2*$^{-/-}$ VE cells, we stained whole embryos with Alexa488-phalloidin and visualized actin filaments in VE cells using a confocal microscope. As predicted from the above findings, the amounts of polymerized actin (observed as the phalloidin staining intensity in confocal microscopy) appeared to be reduced throughout *Enpp2*$^{-/-}$ VE cells compared with those in the wild-type VE cells (Fig. 6A). To exclude the possibility that the differences in the staining intensity resulted from the difference in the Alexa488-phalloidin permeability, we performed the staining using the sections of the yolk sac. In this experiment, to compare the signals precisely, we obtained the fluorescence images using a confocal microscope with constant scanning parameters. As shown in Figure 6B, phalloidin staining

intensity was lower in the *Enpp2*$^{-/-}$ VE cells than that in the wild-type cells. Statistical analysis of the fluorescence intensity in the yolk sac sections indicated that the amounts of polymerized actin were significantly lower in *Enpp2*$^{-/-}$ VE cells than those in wild-type VE cells (Fig. 6C).

Next, we examined whether actin polymerization in VE cells were regulated by the LPA receptor-Rho-ROCK-LIMK pathway. We cultured wild-type mouse embryos with the inhibitors used in the above experiments for 1 day and performed phalloidin staining. As a result, all the drugs that induced the reduction of the lysosome size (Ki16425, C3 exoenzyme, H1152, and S3 peptide) resulted in reductions in phalloidin staining in VE cells (Fig. 6D). Thus, the amount of polymerized actin was reduced in *Enpp2*$^{-/-}$ VE cells most likely as a result of the decrease in the LPA receptor-Rho-ROCK-LIMK signaling.

The above findings suggest the possibility that actin filaments regulate lysosome formation in VE cells. To test this, we examined directly whether perturbation of actin cytoskeleton dynamics causes defects in lysosomes. First, to induce actin-depolymerized conditions similar to those in *Enpp2*$^{-/-}$ VE cells, E7.5 embryos were cultured with 0.3 μM cytochalasin B for 1 day. This treatment led to a significant reduction in lysosome size in VE cells (Fig. 7A), suggesting that actin polymerization is required to form large lysosomes. Moreover, when the embryos cultured with cytochalasin B for 1 day were observed after the drug was removed, the lysosome sizes in VE cells returned to normal over time (Fig. 7B). This finding indicates that the effects of cytochalasin B on lysosomes were reversible and not merely cytotoxic actions. Reversely, stabilization of actin filaments by culturing embryos with 10 nM jasplakinolide also induced reduction in lysosome size (Fig. 7A). Thus, actin depolymerization is also required for lysosome formation. Taken together, these findings suggest that the dynamic regulation of actin turnover is required for the formation of large lysosomes in VE cells, whilst actin filaments tend to shift to the net depolymerization owing to the activation of cofilin as a result of steady-state dephosphorylation of cofilin in *Enpp2*$^{-/-}$ VE cells.

Electroporation of Dominant-Negative Forms of Rho, ROCK, or LIMK Induces Lysosomal Defects in VE Cells—Finally, we tested the validity of our pharmacological experiments using a molecular approach: we overexpressed DN or CA forms of Rho, ROCK, LIMK, or cofilin in VE cells, and observed the changes in lysosome size. For this purpose, we developed a method to introduce exogenous DNAs into VE cells by electroporation (see details in EXPERIMENTAL PROCEDURES). The DN forms used were RhoB (T19N), ROCK (KD-IA), LIMK1 (D460A), and cofilin (S3E), whereas the CA forms used were RhoB (G14V), RCOK (Δ3), LIMK1 (T508EE), and cofilin (S3A) (19-23). To label the electroporated cells, Rho and LIMK cDNAs were subcloned into an pEGFP-IRES vector, whereas ROCK and cofilin were fused to EGFP and YFP, respectively.

We first examined whether inhibition of the Rho-ROCK-LIMK pathway by electroporating their DN forms induced depolymerization of actin filaments. After E7.5 whole embryos were dissected and electroporated, they were cultured for 1 day using an ex vivo whole embryo culture system, and subsequently stained with Alexa546-phalloidin. When EGFP alone was electroporated, phalloidin staining intensity was not changed (Figure 8A), indicating that neither electroporation nor EGFP overexpression affected actin polymerization. In contrast, electroporation of DN-Rho, DN-ROCK, or DN-LIMK induced actin depolymerization (Figure 8A), indicating that the Rho-ROCK-LIMK pathway was inhibited by the electroporation of these expression constructs.

Next, we examined the effects of Rho-ROCK-LIMK inhibition on lysosome formation using LysoTracker Red staining. Electroporation of EGFP alone showed no obvious effects on lysosome size, whereas electroporation of DN-Rho, DN-ROCK, or DN-LIMK induced size

reduction of lysosomes in VE cells (Figure 8B-C). In severe cases (10%-20%), LysoTrakcer Red staining disappeared (data not shown, Figure 8C). Inhibition of Rho-ROCK-LIMK pathway results in the decrease of cofilin phosphorylation, thus leading to activation of cofilin. To mimic this, we used the S3A mutant of cofilin, which is constitutively active and cannot be phosphorylated. Electroporation of cofilin (S3A) induced the size reduction of lysosomes, although the steady state levels of phalloidin-staining intensity were not apparently changed (Figure 8). Thus, these findings demonstrate that inhibition of the Rho-ROCK-LIMK-cofilin signaling pathway led to defects in the formation of large lysosomes in VE cells.

Next, we examined the effects of Rho-ROCK-LIMK activation on lysosome formation. When the CA forms of Rho or LIMK were electroporated, actin polymerization was increased (Figure S6A), indicating that Rho and LIMK were activated in VE cells by electroporation of these CA constructs. CA-Rho and CA-LIMK led to the reduction of lysosome size in VE cells (Figure S6B-C), suggesting that activation of Rho or LIMK resulted in the defects in lysosome formation. When CA-ROCK was electroporated, VE cells became severely deformed and were unsuitable for further examination (data not shown). We thus excluded CA-ROCK electroporation from the analysis. Activation of the Rho-ROCK-LIMK pathway phosphorylates cofilin, thereby leading to inactivation of cofilin. To induce this state, we used the S3E mutant of cofilin, which mimics the phosphorylated state of cofilin. When cofilin (S3E) was electroporated, lysosomes became smaller, although the changes in the steady state levels of phalloidin staining were not apparent (Figure S6B-C). These findings suggest that overactivation of the Rho-ROCK-LIMK-cofilin pathway led to the defects in lysosome formation. Thus, the balance between actin polymerization and depolymerization was important to maintain the large size of lysosomes in VE cells, compatible with our findings that both cytochalasin B and jasplakinolide led to lysosomeal defects.

DISCUSSION

In this study, we demonstrated that autotaxin-LPA signaling is required to form distinctive large lysosomes in yolk sac VE cells. We provided the evidence that constitutive activation of LPA receptors as a result of high *Enpp2* expression in the yolk sac VE cells, starting from E7.5, is required for the formation of large lysosomes. We also showed that actin turnover dynamics regulated by the Rho-ROCK-LIMK pathway play a central role in the downstream pathway.

We found linkage between autotaxin-LPA signaling and lysosome biogenesis. Although little is known about the relationship between LPA and organelle biogenesis, multiple roles of Rho GTPases, the main downstream effectors of LPA signaling, in endocytic trafficking have been reported (30, 31). For example, RhoB and RhoD, GTPases known to associate with endosomes, control endocytic trafficking by regulating actin polymerization (30 31). The interaction of RhoB and mDia2 on endosomes regulates vesicle trafficking by controlling actin dynamics (32). Our findings demonstrate that inhibition of Rho and its downstream signaling pathway by pharmacological blockers or electroporation of DN constructs led to fragmentation of lysosomes in VE cells. Thus, our results suggest that extracellular production of LPA by autotaxin in mouse embryos controls endocytic vesicle trafficking through the Rho pathway to form large lysosomes in yolk sac VE cells. This notion is compatible with a previous argument that the phenotypes of *Enpp2*$^{-/-}$ embryos are similar to those of embryos lacking $G\alpha_{12}$ and $G\alpha_{13}$, the key mediators for the Rho pathway (10, 33).

We also showed linkage between autotaxin and actin dynamics. Although it is well known that LPA regulates actin cytoskeleton rearrangements, ours is the first study to indicate that autotaxin controls the levels of actin polymerization in vivo. Because autotaxin protein was detected in the ECF (Figure 1D), autotaxin should produce

LPA and activate LPA receptors constantly in mouse embryos, thereby controlling actin dynamics required for large lysosome formation in VE cells. In addition to the well-studied roles of actin in endocytosis (34-36), accumulating evidence has suggested that actin directly regulates vesicle fusion and transport in the endocytic pathway (34, 35). For example, treatment of cells with actin-depolymerizing drugs induced defects in the transport from late endosomes to lysosomes in mammalian cells (37, 38). In addition, in vitro fusion assays showed that actin facilitated fusion between phagosomes and late endosomes and between late endosomes themselves (39). Thus, autotaxin appears to promote vesicle fusion and/or transport processes from endosomes to lysosomes in VE cells. Future studies are required to examine whether and how autotaxin-LPA controls endocytic vesicle trafficking.

VE cells and yeast have many common features in endocytic vesicles. First, both are active in endocytosis/digestion and have large lysosomes (vacuoles). Second, Rho activity is required for lysosome (vacuole) formation: two Rho GTPases, Rho1p and Cdc42p, are enriched on vacuole membranes and required for docking and fusion of vacuoles in yeast (40), whereas in VE cells, C3 exotoxin and DN-Rho induced fragmentation of lysosomes. Third, actin is involved in lysosome formation: actin was bound to vacuoles, and vacuole fusion was inhibited by jasplakinolide or an actin-destabilizing reagent, latrunculin, in yeast (41), whereas cytochalasin B or jasplakinolide inhibited lysosome formation in VE cells. Therefore, there seems to be a common cellular machinery to maintain large lysosomes in these cells. We tried to enlarge lysosomes in cultured cell lines by treating them with LPA, by overexpressing *Enpp2*, or by transfecting CA forms of Rho, ROCK, or LIMK, but we could not see any changes in lysosome size (S. K. and M. M., unpublished observation). Thus, to make such large lysosomes (vacuoles) as observed in VE cells and yeast, sufficient amounts of certain cellular components required for lysosome biogenesis may be necessary in addition to the activation of Rho signaling and actin dynamics. Conversely, we tried to reduce the size of lysosomes in cultured cell lines by treating them with LPA antagonists or by transfecting DN forms of Rho, ROCK, or LIMK. However, we did not see any apparent changes of lysosome size in VE cells (S. K. and M. M., unpublished observation), although we could not evaluate the lysosome size correctly because lysosomes in cultured cell lines were much smaller than those in VE cells.

In summary, we have found a novel function of autotaxin-LPA signaling in the regulation of lysosome biogenesis. Further studies are required to examine whether autotaxin-LPA controls actin dynamics and lysosome formation in other *Enpp2*-expressing cells, exactly which processes in lysosome biogenesis are regulated by autotaxin-LPA, and what biological significance can be attributed to the autotaxin-LPA signaling in lysosome formation. It is also worth noting that yolk sac VE cells provide a useful system to study the cellular and molecular mechanisms of vesicle trafficking and biogenesis in mammalian cells because of the simple anatomy of the yolk sac, the large size and easy labeling of endocytic vesicles, and their accessibility for pharmacological manipulation and a molecular approach.

REFERENCES

1. Stefan, C., Jansen, S., and Bollen, M. (2005) *Trends Biochem. Sci.* **30**, 542-550
2. Tokumura, A., Majima, E., Kariya, Y., Tominaga, K., Kogure, K., Yasuda, K., and Fukuzawa, K. (2002) *J. Biol. Chem.* **277**, 39436-39442

3. Umezu-Goto, M., Kishi, Y., Taira, A., Hama, K., Dohmae, N., Takio, K., Yamori, T., Mills, G. B., Inoue, K., Aoki, J., and Arai, H. (2002) *J. Cell Biol.* **158**, 227-233
4. van Meeteren, L. A., and Moolenaar, W. H. (2007) *Prog. Lipid Res.* **46**, 145-160
5. Anliker, B., and Chun, J. (2004) *Semin. Cell Dev. Biol.* **15**, 457-465
6. Birgbauer, E., and Chun, J. (2006) *Cell. Mol. Life Sci.* **63**, 2695-270
7. Meyer zu Heringdorf, D., and Jakobs, K. H. (2007) *Biochim. Biophys. Acta* **1768**, 923-940
8. Clair, T., Aoki, J., Koh, E., Bandle, R. W., Nam, S. W., Ptaszynska, M. M., Mills, G. B., Schiffmann, E., Liotta, L. A., and Stracke, M. L. (2003) *Cancer Res.* **63**, 5446-5453
9. Tanaka, M., Okudaira, S., Kishi, Y., Ohkawa, R., Iseki, S., Ota, M., Noji, S., Yatomi, Y., Aoki, J., and Arai. H. (2006) *J. Biol. Chem.* **281**, 25822-25830
10. van Meeteren, L. A., Ruurs, P., Stortelers, C., Bouwman, P., van Rooijen, M. A., Pradere, J. P., Pettit, T. R., Wakelam, M. J., Saulnier-Blache, J. S., Mummery, C. L., Moolenaar, W. H., and Jonkers, J. (2006) *Mol. Cell. Biol.* **26**, 5015-5022
11. Bielinska, M., Narita, N., and Wilson, D. B. (1999) *Int. J. Dev. Biol.* **43**, 183-205
12. Jollie, W. P. (1990) *Teratol.* **41**, 361-381
13. Lloyd, J. B. (1990) *Teratol.* **41**, 383-393
14. Luzio, J. P., Pryor, P. R., and Bright, N. A. (2007) *Nat. Rev. Mol. Cell Biol.* **8**, 622-632
15. Mullins, C., and Bonifacino, J. S. (2001) *BioEssays* **23**, 333-343
16. Koike, S., Keino-Masu, K., Ohto, T., and Masu, M. (2006) *Genes Cells* **11**, 133-142
17. Osumi-Yamashita, N., Ninomiya, Y., Doi, H., and Eto, K. (1994) *Dev. Biol.* **164**, 409-419
18. Tam, P. P. (1998) *Int. J. Dev. Biol.* **42**, 895-902
19. Kamon, H., Kawabe, T., Kitamura, H., Lee, J., Kamimura, D., Kaisho, T., Akira, S., Iwamatsu, A., Koga, H., Murakami, M., and Hirano, T. (2006) *EMBO J.* **25**, 4108-4119
20. Ishizaki, T., Naito, M., Fujisawa, K., Maekawa, M., Watanabe, N., Saito, Y., and Narumiya, S. (1997) *FEBS Lett.* **404**, 118-124
21. Ohashi, K., Nagata, K., Maekawa, M., Ishizaki, T., Narumiya, S., and Mizuno, K. (2000) *J. Biol. Chem.* **275**, 3577-3582
22. Kaji, N., Ohashi, K., Shuin, M., Niwa, R., Uemura, T., and Mizuno, K. (2003) *J. Biol. Chem.* **278**, 33450-33455
23. Yang, N., Higuchi, O., Ohashi, K., Nagata, K., Wada, A., Kangawa, K., Nishida, E., and Mizuno, K. (1998) *Nature* **393**, 809-812
24. Ohta, H., Sato, K., Murata, N., Damirin, A., Malchinkhuu, E., Kon, J., Kimura, T., Tobo, M., Yamazaki, Y., Watanabe, T., Yagi, M., Sato, M., Suzuki, R., Murooka, H., Sakai, T., Nishitoba, T., Im, D. S., Nochi, H., Tamoto, K., Tomura, H., and Okajima, F. (2003) *Mol. Pharmacol.* **64**, 994-1005
25. Davis, M. D., Clemens, J. J., Macdonald, T. L., and Lynch, K. R. (2005) *J. Biol. Chem.* **280**, 9833-9841
26. Maekawa, M., Ishizaki, T., Boku, S., Watanabe, N., Fujita, A., Iwamatsu, A., Obinata, T., Ohashi, K., Mizuno, K., and Narumiya, S. (1999) *Science* **285**, 895-898
27. Van Troys, M., Huyck, L., Leyman, S., Dhaese, S., Vandekerkhove, J., and Ampe, C. (2008) *Eur. J. Cell Biol.* **87**, 649-667
28. Amano, M, Fukuta, Y., and Kaibuchi, K. (2000) *Exp. Cell Res.* **261,** 44-51

29. Aizawa, H., Wakatsuki, S., Ishii, A., Moriyama, K., Sasaki, Y., Ohashi, K., Sekine-Aizawa, Y., Sehara-Fujisawa, A., Mizuno, K., Goshima, Y., and Yahara, I. (2001) *Nat. Neurosci.* **4**, 367-373
30. Qualmann, B., and Mellor, H. (2003) *Biochem. J.* **371**, 233-241
31. Symons, M., and Rusk, N. (2003) *Curr. Biol.* **13**, R409-418
32. Wallar, B. J., Deward, A. D., Resau, J. H., and Alberts, A. S. (2007) *Exp. Cell Res.* **313**, 560-571
33. Gu, J. L., Muller, S., Mancino, V., Offermanns, S., and Simon, M. I. (2002) *Proc. Natl. Acad. Sci. U. S. A.* **99**, 9352-9357
34. Engqvist-Goldstein, A. E., and Drubin, D. G. (2003) *Annu. Rev. Cell Dev. Biol.* **19**, 287-332.
35. Girao, H., Geli, M. I., and Idrissi, F. Z. (2008) *FEBS Lett.* **582**, 2112-2119
36. Smythe, E., and Ayscough, K. R. (2006) *J. Cell Sci.* **119**, 4589-4598
37. Barois, N., Forquet, F., and Davoust, J. (1998) *J. Cell Sci.* **111**, 1791-1800
38. van Deurs, B., Holm, P. K., Kayser, L., and Sandvig, K. (1995) *Eur. J. Cell Biol.* **66**, 309-323
39. Kjeken, R., Egeberg, M., Habermann, A., Kuehnel, M., Peyron, P., Floetenmeyer, M., Walther, P., Jahraus, A., Defacque, H., Kuznetsov, S. A., and Griffiths, G. (2004) *Mol. Biol. Cell* **15**, 345-335
40. Eitzen, G., Thorngren, N., and Wickner, W. (2001) *EMBO J.* **20**, 5650-5656
41. Eitzen, G., Wang, L., Thorngren, N., and Wickner, W. (2002) *J. Cell Biol.* **158**, 669-679

FOOTNOTES

This work was supported in part by Grants-in-Aid for Scientific Research on Priority Areas and the 21st Century COE Program from the Ministry of Education, Culture, Sports, Science, and Technology of Japan, and grants from the Mitsubishi Foundation and the NOVARTIS Foundation (Japan).

Acknowledgements—The authors thank Drs. R. Kageyama, N. Osumi, K. Mizuno, K. Ohashi, S. Hirano, and S. Narumiya for reagents, protocols, and advice; K. Yagami, N. Kajiwara, K. Nakao, J. Sakamoto, and Y. Ohno for technical support; H. Bito, K. Kaibuchi, K. Nakayama, M. Yamamoto, T. Okada, K. Irie, and F. Miyamasu for useful comments.

The abbreviations used are: CA, constitutive active; DMEM, Dulbecco's modified Eagle medium; DN, dominant negative; E, embryonic day; EGFP, enhanced green fluorescent protein; ENPP2, ectonucleotide pyrophosphatase/phosphodiesterase 2; Gapdh, glyceraldehyde-3-phosphate dehydrogenase; HRP, horse radish peroxidase ; LIMK, LIM kinase; LPA, lysophosphatidic acid; LysoPLD, lysophospholipase D; MAPK, mitogen-activated protein kinase; MLC, myosin light chain; PBS, phosphate-buffered saline; PI3K, phosphatidylinositol 3-kinase; PLC, phospholipase C; PTX, pertussis toxin; ROCK, Rho-associated coiled-coil containing protein kinase; RT-PCR, reverse transcriptase-polymerase chain reaction; S1P, sphingosine 1-phosphate; VE, visceral endoderm.

FIGURE LEGENDS

FIGURE 1. **Targeted disruption of the murine *Enpp2* gene.** A, scheme of targeting strategy. Part of exon 6 and the entirety of exon 7 of the *Enpp2* gene were replaced with a stop-*IRES-lacZ-polyA-pgk-Neo* cassette. Abbreviations: DTA, diphtheria toxin A fragment; H, *Hpa*I; P, *Pvu*II, S, *Sac*I. B, Southern blotting of *Hpa*I-, *Pvu*II-, or *Sac*I-digested genomic DNA hybridized with 5', 3', or neo probes verified the germline transmission of the correctly targeted *Enpp2* allele. Closed and open

arrowheads indicate the bands for wild-type and targeted alleles, respectively. The band sizes of the wild-type and targeted alleles are 8.6 kb and 6.8 kb for the 5' probe, and 7.0 kb and 4.5 kb for the 3' probe, respectively. C, RT-PCR analysis revealed that *Enpp2* mRNA was absent in the *Enpp2*$^{-/-}$ embryos. RT(-) indicates a control reaction without reverse transcriptase. D, western blot revealed that autotaxin protein was absent in the extraembryonic coelomic fluid of the E8.5 *Enpp2*$^{-/-}$ embryos. WT indicates *Enpp2*$^{+/+}$ or *Enpp2*$^{+/-}$ control embryos (denoted in the same way hereafter). E, appearance of the E9.5 yolk sac. Large vitelline vessels formed in the control (black arrow) but not in the *Enpp2*$^{-/-}$ yolk sac, in which red blood cells precipitated (white arrows). F, gross appearance of the E9.5 embryos. Most *Enpp2*$^{-/-}$ embryos were much smaller than the controls and did not undergo embryonic turning. The arrow indicates the head cavity in *Enpp2*$^{-/-}$ embryos. Scale bar represents 1.0 mm.

FIGURE 2. ***Enpp2* mRNA is highly expressed in yolk sac VE cells.** A, in situ hybridization of *Enpp2*. Strong expression was observed in the embryonic ectoderm (ect) at E6.0-E6.5, in the yolk sac (ys) at E7.5-E8.5, and in the head fold (hf) and somites (arrowheads) at E8.5. Transverse sections (bottom) showed robust expression in the visceral endoderm (ve) of the yolk sac. Abbreviations: epc, ectoplacental cone; hp, head process; mes, extraembryonic mesoderm. Scale bar represents 190 μm (top left), 210 μm (top right), 400 μm (middle left), 450 μm (middle right), 270 μm (bottom left), and 40 μm (bottom right). B, RT-PCR of *Enpp2* mRNA in the E7.0-E12.5 yolk sac. RT(-) indicates a control reaction without reverse transcriptase. Glyceraldehyde-3-phosphate dehydrogenase *(Gapdh)* was used as a control.

FIGURE 3. **Formation of large lysosomes is impaired in the yolk sac VE cells of *Enpp2*$^{-/-}$ embryos.** A, IgG immunostaining (top), electron microscopy (middle), and LysoTracker Red staining (bottom) of the E8.5 yolk sac. Immunostaining with anti-mouse IgG antibody detects endocytic vesicles in the VE cells (ve). IgG-containing vesicles in *Enpp2*$^{-/-}$ VE cells were smaller than those in the wild-type (WT) cells. Electron microscopy showed a few large vesicles in the apical portion of the wild-type VE cells (arrows), whereas numerous vesicles of smaller size were seen in the *Enpp2*$^{-/-}$ cells (arrows). Confocal microscopic images of the yolk sac showed that LysoTracker Red-positive lysosomes were decreased in size but increased in number in the *Enpp2*$^{-/-}$ VE cells compared with those in the control. The yellow dotted lines indicate the boundary of VE cells. Scale bar represents 20 μm (top), 1.7 μm (middle), and 12 μm (bottom). Abbreviations: bc, blood cells; mv, microvillus; n, nucleus. B, the size and number of lysosomes in VE cells. Lysosomes were significantly decreased in size and increased in number in *Enpp2*$^{-/-}$ VE cells. The values are the means ± S.E.M. (***$P < 0.001$; unpaired t-test). The number of embryos examined is shown in each column.

FIGURE 4. **Blockade of the LPA receptor-Rho-ROCK-LIMK pathway induces defects in lysosome formation.** A, confocal microscopic images of the yolk sac stained with LysoTracker Red. After E7.5 wild-type embryos were cultured with an LPA_1/LPA_3 antagonist (10 μM Ki16425) or an $S1P_1/S1P_3$ antagonist (10 μM VPC23019) for 1 day, LysoTracker Red staining was performed. Ki16425 induced the size reduction of lysosomes in the VE cells, whereas VPC23019 was ineffective. Scale bar represents 6 μm. B-E, quantitation of the lysosome size in the embryos cultured with the indicated inhibitors. Treatment of wild-type embryos with Ki16425 (Ki) as well as the inhibitors of Rho (20 μg/ml C3 exoenzyme), ROCK (0.1 μM H1152), or LIMK (15 μg/ml S3 peptide) resulted in significant size reduction in lysosomes when compared with the controls, whereas treatment with VPC23019 (VPC) and the inhibitors for G_i (0.5 μg/ml pertussis toxin (PTX)), PLC (10 μM U-73122), PI3K (10 μM LY294002), MAPK (10 μM PD98059), or myosin II (10 μM blebbistatin) showed no effect on the

size of lysosomes. The values are the means ± S.E.M. [*$P < 0.05$, **$P < 0.01$; ANOVA with a Tukey-Kramer post-hoc test (B-C), unpaired t-test (D-E)]. The number of embryos examined is shown in each column.

FIGURE 5. **Phosphorylation of cofilin is decreased in *Enpp2*$^{-/-}$ VE cells.** A, confocal microscopic images of the yolk sac stained with anti-phosphorylated-cofilin (P-cofilin) or anti-total-cofilin (red). E-cadherin immunostaining (E-cad, green) shows the cell boundaries. Scale bar represents 4 μm. B, intensity of the immunostaining. Staining intensity for phosphorylated cofilin, measured in 3 different regions (36.6 x 36.6 μm) per embryo, was significantly reduced in *Enpp2*$^{-/-}$ VE cells, whereas staining intensity of total cofilin and E-cadherin was unchanged. The values are the means ± S.E.M. (*$P < 0.05$; unpaired t-test). The number of embryos examined is shown in each column.

FIGURE 6. **Polymerized actin is reduced in *Enpp2*$^{-/-}$ VE cells.** A, confocal microscopic images of the VE cells stained with Alexa488-phalloidin. Top, middle, and bottom panels show the superficial, intermediate, and deep layers of the apical portion of the VE cells, respectively. Phalloidin staining was reduced throughout all layers in *Enpp2*$^{-/-}$ VE cells. B, Alexa488-phalloidin staining of the cryostat sections of E8.5 yolk sacs. The apical portion is at the top. Bottom figures show higher power images of VE cells. Abbreviations: bc, blood cells; ve, visceral endoderm cells. C, the cumulative plot shows that phalloidin staining intensity was lower in *Enpp2*$^{-/-}$ VE cells than that in wild-type VE cells. D, Phalloidin staining after inhibitor treatment. After wild-type embryos were cultured in the presence of the indicated inhibitors for 1 day, Alexa488-phalloidin staining was performed. Treatment with Ki16425, C3 exoenzyme, H1152, or S3 peptide, but not with VPC23019, led to the reduction of phalloidin staining in VE cells. Scale bar represents 6 μm (A, D), 40 μm (B, top), and 4 μm (B, bottom).

FIGURE 7. **Actin inbibitors induce defects in lysosome formation.** A, quantitation of the lysosome size in the embryos cultured with the indicated inhibitors. After E7.5 wild-type embryos were cultured with 0.3 μM cytochalasin B (CB, a cell-permeable inhibitor of actin polymerization) or 10 nM jasplakinolide (Jasp, a cell-permeable stabilizer of actin filament) for 1 day, LysoTracker Red staining was performed. Both actin inhibitors induced the size reduction in lysosomes in VE cells. B, recovery of the lysosome size after washout of cytochalasin B. After E7.5 wild-type embryos were cultured with 0.3 μM cytochalasin B for 1 day, the drug was removed. LysoTracker Red staining was performed 5, 30, and 60 min after washout of cytochalasin B. The lysosome size increased over time. The values are the means ± S.E.M. (*$P < 0.05$, **$P < 0.01$, ***$P < 0.001$; ANOVA with a Tukey-Kramer post-hoc test). The number of embryos examined is shown in each column.

FIGURE 8. **Electroporation-mediated inhibition of the Rho-ROCK-LIMK pathway induces lysosomal defects in VE cells.** A-B, confocal microscopic images of the VE cells stained with Alexa546-phalloidin (A) or LysoTracker Red (B). After whole embryos were electroporated with the expression constructs for the indicated molecules and cultured for 1 day, they were stained with Alexa546-phalloidin or LysoTracker Red. To identify electroporated cells, EGFP was co-expressed by subcloning into a pEGFP-IRES2 vector or making EGFP (or YFP) fusion proteins. Asterisks indicate electroporated cells. DN-Rho, DN-ROCK, or DN-LIMK induced the decrease in phalloidin staining, whereas elecroporation of EGFP alone had no effect (A). In the VE cells expressing DN-Rho, DN-ROCK, DN-LIMK, or cofilin (S3A), lysosomes became smaller or LysoTracker Red staining disappeared. The cells that showed severe morphological abnormalities were excluded from the analyses. Scale bars indicate 10 μm. C, summary of the effects of DN-Rho, DN-ROCK, DN-LIMK, and cofilin (S3A) on

lysosome size. The VE cells possessing at least 1 lysosome with an area of more than 40 μm^2 were categorized as "normal," whereas those possessing only small lysosomes (area smaller than 40 μm^2) were categorized as "small." The cells showing no visible LysoTracker Red staining were categorized as having "no signal." The numbers of the VE cells examined are shown on the right.

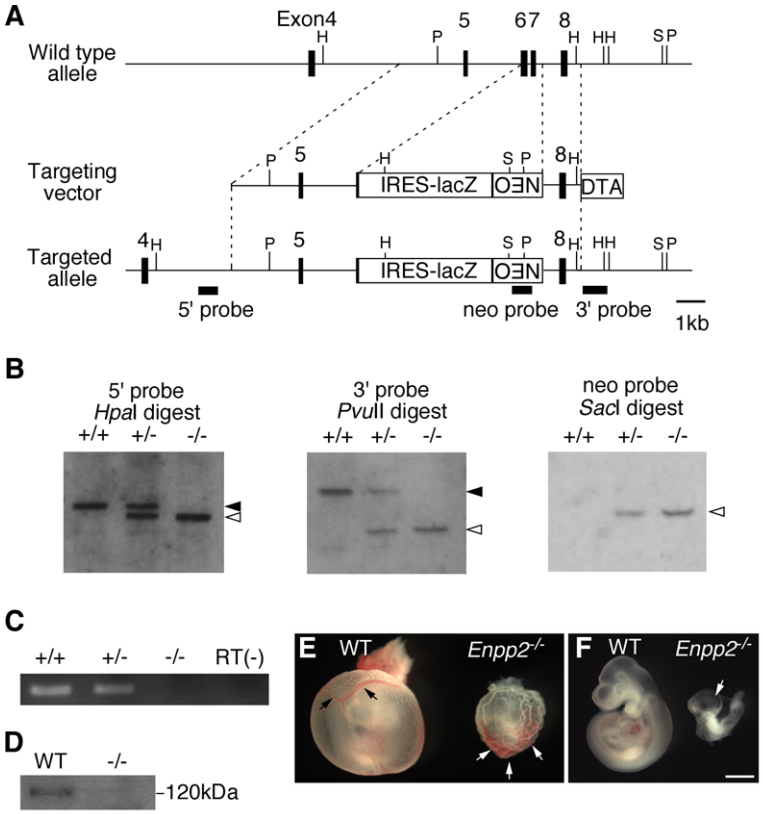
A
Exon4
5
67
8
Wild type allele
H
P
H HH
S P
Targeting vector
IRES-lacZ
NEO
DTA
Targeted allele
4H
5' probe
neo probe
3' probe
1kb
B
5' probe
HpaI digest
+/+ +/- -/-
3' probe
PvuII digest
neo probe
SacI digest
C
+/+ +/- -/- RT(-)
D
WT -/-
120kDa
E WT Enpp2-/-
F WT Enpp2-/-

Figure 1

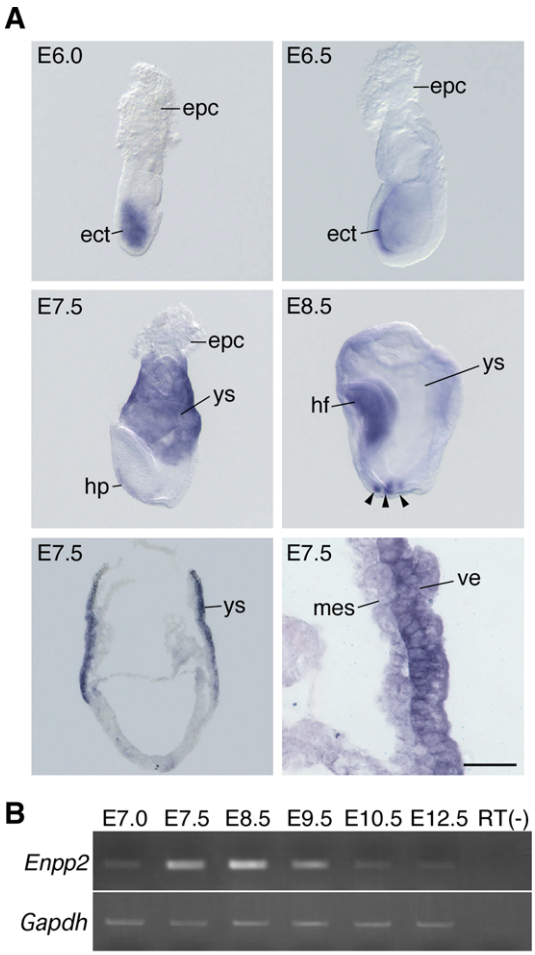
A
E6.0
epc
ect
E6.5
epc
ect
E7.5
epc
ys
hp
E8.5
ys
hf
E7.5
ys
E7.5
ve
mes
B
E7.0 E7.5 E8.5 E9.5 E10.5 E12.5 RT(-)
Enpp2
Gapdh

Figure 2

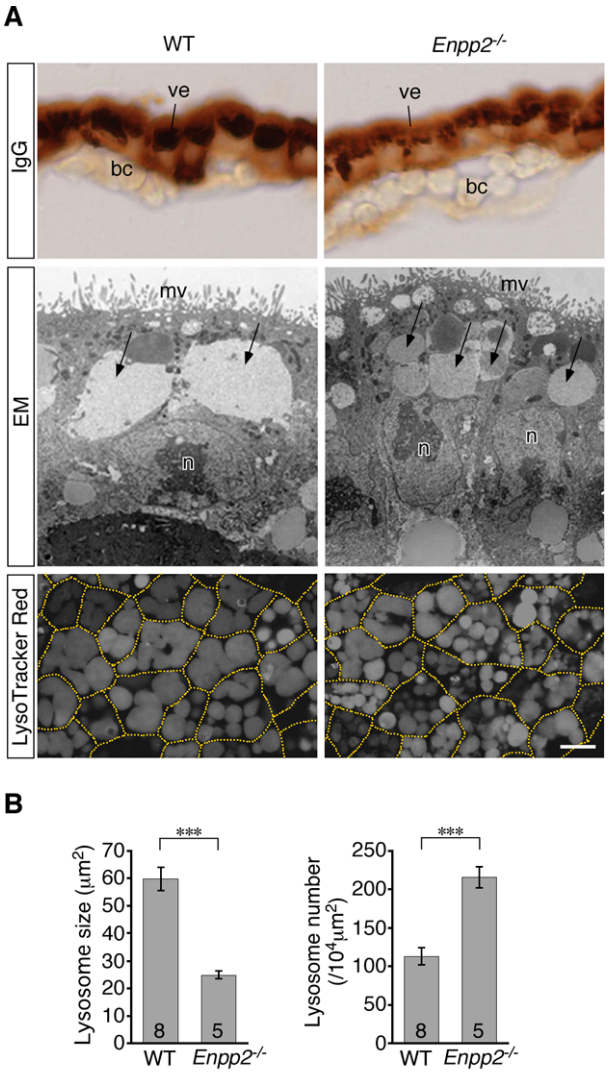
A
WT
Enpp2-/-
IgG
ve
bc
ve
bc
EM
mv
n
mv
n
n
LysoTracker Red
B
***
Lysosome size (μm2)
70
60
50
40
30
20
10
0
8
5
WT
Enpp2-/-
***
Lysosome number (/10⁴μm2)
250
200
150
100
50
0
8
5
WT
Enpp2-/-

Figure 3

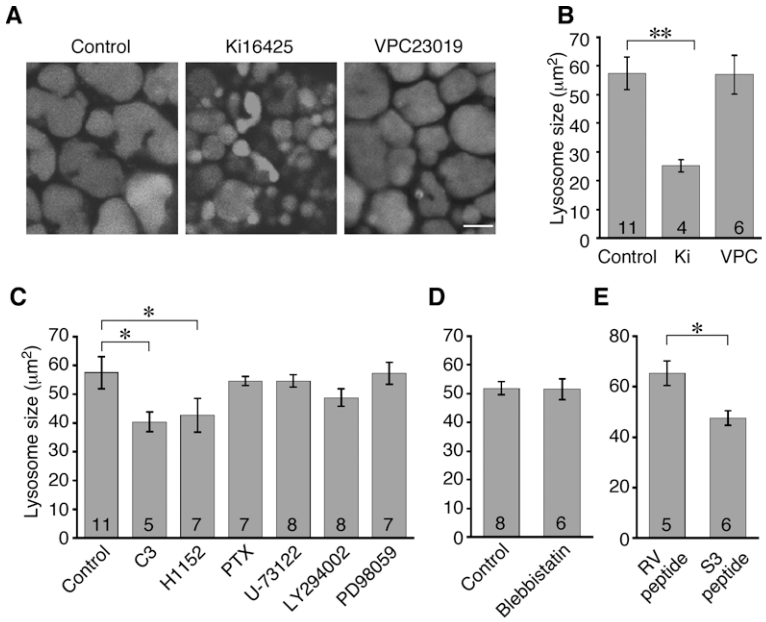
A
Control
Ki16425
VPC23019
B
Lysosome size (μm²)
**
11
4
6
Control
Ki
VPC
C
Lysosome size (μm²)
*
*
11
5
7
7
8
8
7
Control
C3
H1152
PTX
U-73122
LY294002
PD98059
D
8
6
Control
Blebbistatin
E
*
5
6
RV peptide
S3 peptide

Figure 4

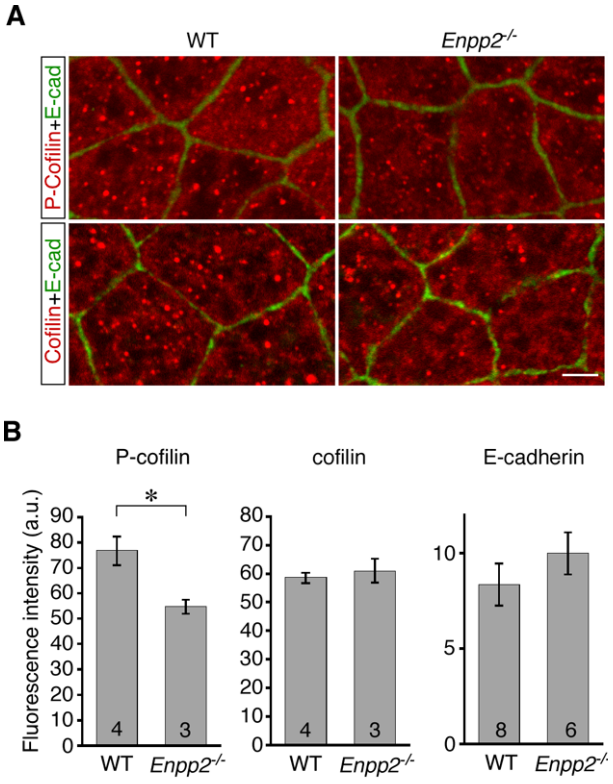
A
WT
Enpp2-/-
P-Cofilin+E-cad
Cofilin+E-cad
B
P-cofilin
cofilin
E-cadherin
Fluorescence intensity (a.u.)
*
WT
Enpp2-/-

Figure 5

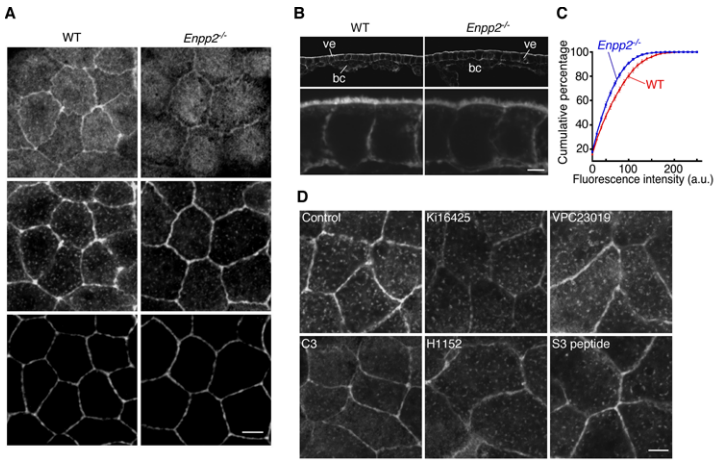
A
WT
Enpp2-/-
B
WT
Enpp2-/-
ve
bc
ve
bc
C
Enpp2-/-
WT
Cumulative percentage
100
80
60
40
20
0
100
200
Fluorescence intensity (a.u.)
D
Control
Ki16425
VPC23019
C3
H1152
S3 peptide

Figure 6

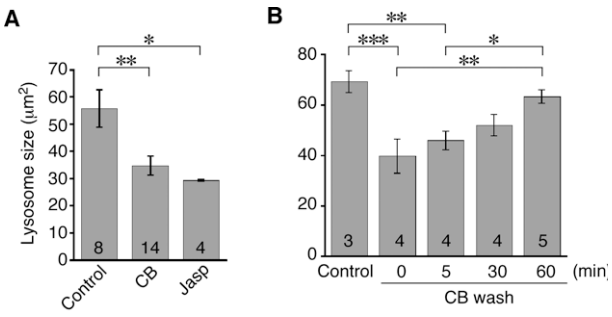
A
B
Lysosome size (μm²)
70
60
50
40
30
20
10
0
8
14
4
Control
CB
Jasp
*
**
80
60
40
20
0
3
4
4
4
5
Control
0
5
30
60
(min)
CB wash
**
***
*
**

Figure 7

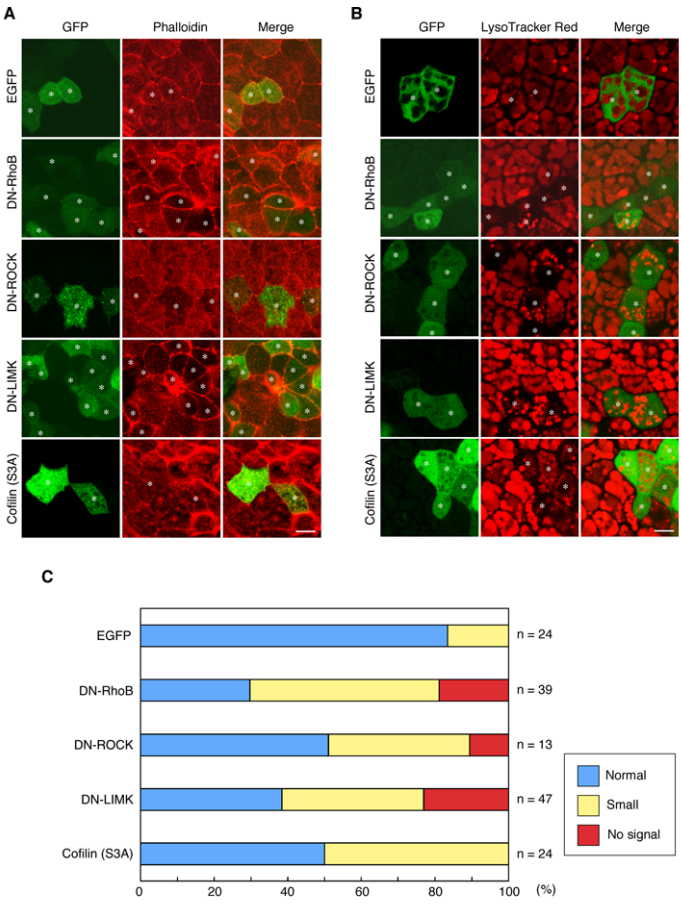
A
GFP
Phalloidin
Merge
EGFP
DN-RhoB
DN-ROCK
DN-LIMK
Cofilin (S3A)
B
GFP
LysoTracker Red
Merge
EGFP
DN-RhoB
DN-ROCK
DN-LIMK
Cofilin (S3A)
C
EGFP
DN-RhoB
DN-ROCK
DN-LIMK
Cofilin (S3A)
n = 24
n = 39
n = 13
n = 47
n = 24
Normal
Small
No signal
0
20
40
60
80
100
(%)

Figure 8